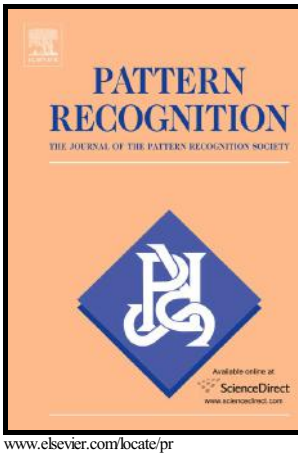

www.elsevier.com/locate/pr

Breast Cancer Detection Using MRF-based Probable Texture Feature and Decision-level Fusion-based Classification using HMM on Thermography Images

Rozita Rastghalam, Hossein Pourghassem

PII: S0031-3203(15)00340-4
DOI: http://dx.doi.org/10.1016/j.patcog.2015.09.009
Reference: PR5513

To appear in: *Pattern Recognition*

Received date: 14 July 2014
Revised date: 16 August 2015
Accepted date: 15 September 2015

Cite this article as: Rozita Rastghalam and Hossein Pourghassem, Breast Cance Detection Using MRF-based Probable Texture Feature and Decision-leve Fusion-based Classification using HMM on Thermography Images, *Patter Recognition,* http://dx.doi.org/10.1016/j.patcog.2015.09.009

Breast Cancer Detection Using MRF-based Probable Texture Feature and Decision-level Fusion-based Classification using HMM on Thermography Images

Rozita Rastghalam[1], Hossein Pourghassem[2]
[1, 2,] Department of Electrical Engineering, Najafabad Branch, Islamic Azad University, Najafabad, Isfahan, Iran.

Corresponding author:
Hossein Pourghassem,
Department of Electrical Engineering, Najafabad Branch, Islamic Azad University, Najafabad, Isfahan, Iran.
Email: h_pourghasem@iaun.ac.ir

Phone number: 0098 31 42291111, fax number: 0098 31 42291017.

Abstract

Breast cancer is one of the major causes of death for women in the last decade. Thermography is a breast imaging technique that can detect cancerous masses much faster than the conventional mammography technology. In this paper, a breast cancer detection algorithm based on asymmetric analysis as primitive decision and decision-level fusion by using Hidden Markov Model (HMM) is

proposed. In this decision structure, by using primitive decisions obtained from extracted features from left and right breasts and also asymmetric analysis, final decision is determined by a new application of HMM. For this purpose, a novel texture feature based on Markov Random Field (MRF) model that is named MRF-based probable texture feature and another texture feature based on a new scheme in Local Binary Pattern (LBP) of the images are extracted. In the MRF-based probable texture feature, we try to capture breast texture information by using proper definition of neighborhood system and clique and also determination of new potential functions. Ultimately, our proposed breast cancer detection algorithm is evaluated on a variety dataset of thermography images and false negative rate of 8.3% and false positive rate of 5% are obtained on test image dataset.

Keywords - Breast cancer, local binary pattern, MRF-based probable texture feature, hidden Markov model, decision-level fusion.

1. INTRODUCTION

One of the most common malignancies and the main reason of death in women aged 45 to 55 is breast cancer. In 2010, the American cancer society announced that breast cancer has been the most common type of cancer amongst women (27%) and a major cause of cancer death among them [1]. There are several imaging techniques to detect breast cancer such as mammography, Magnetic Resonance Imaging (MRI), ultrasound, and thermography. The mammography imaging has some drawbacks such as to be invasive, painful, and improper for women with dense breasts, implants, fibrocystic breasts, or on hormone replacement therapy. However, experts believe that electromagnetic radiation because of the creation of mutations in genes can also be a triggering factor for cancerous growth [2]. Therefore, ultrasound method is recommended for these patients. It is a non-invasive imaging technique that is useful to determine type and form of mass; however this imaging depends on physician experience and knowledge. MRI also as mammography cannot

identify the difference between a cancerous lump and a benign cyst [3, 4]. Digital Infrared Thermal Imaging (DITI) is a non-invasive test in which there is no contact with the body of any kind, no radiation and also the imaging procedure is painless [5]. Researchers have suggested that if tumor is detected very soon in patient breast (tumor size less than 10 mm), the chance of cure will be 85% as opposed to 10% if the cancer is detected lately. Note that the thermography imaging detects tumor 8-10 years earlier than mammography imaging [6].

One of the popular ways for separating the normal from abnormal breast is the application of asymmetric analysis in which the left and right breast features are compared together. In these algorithms, the comparison of left and right breasts is performed based on the extracted features from image or use of pixel temperature as a feature. For example, in [7], difference between histograms of pixel temperature of left and right breasts has been used as a measure for abnormality detection. Qi et al. [8] divided each breast thermography image into four quadrants and compared the mean, standard deviation, median, minimum and maximum temperatures for each quadrant of the breast and then specified the upper outer quadrant of breasts that was the most probable area for tumor growth. More than 1° C temperature difference between mean of each left breast quadrant with the right breast was marked with score 1 and temperature difference between 0.5 to 1 was determined with score 0.5. An index was created by adding the scores of four quadrants and the index greater than 1 indicated the presence of abnormality [9]. In [10], temperature distributions between the left and right breasts and Localized Temperature Increases (LTI) have been considered as a feature related to pixel temperature. LTI has been calculated as difference between the pixel temperature and corresponding background temperature.

In other algorithms that have been proposed to separate the normal from abnormal breasts, there are three major steps as breast segmentation, feature extraction from the segmented regions and classification of breast regions.

One of the useful methods to breast segmentation is done by identifying the left and right body boundaries using Canny or Sobel edge detector or even by using a simple thresholding and finally

two lower curves of the breasts are determined by means Hough Transform [8, 11, 12, 13]. Other techniques such as segmentation-based region growing [14] and Region Of Interest (ROI) cropping [15] have also been presented. In [16, 17], two color segmentation techniques, K-means and fuzzy c-means for regions with high metabolism have been introduced. Moreover, mathematical tools such as graph also have been used for the medical image segmentation. For example, in [18], a robust graph-based segmentation algorithm for the breast mass detection in the ultrasound images has been presented.

The feature extraction is a significant section in all breast cancer detection algorithms. Wavelet transform [19], lyaupon exponent [17], fractal dimension [20], and mutual information [21] have been effective for feature extraction. Utilization of cumulative histogram [22], Bezier histogram [8], the first order moments such as mean, skewness and kurtosis [14, 15, 22], the second order statistical parameters namely co-occurrence matrix [23] are applied to define the features from the breast thermograph. To detect healthy and cancerous cases, different tools such as fuzzy clustering [13], artificial neural network [22], different similarity measures [14, 15, 22, 24] have been applied.

In most of the above works, the aim of researches has been the classification of normal from abnormal images. However, false positive (FP) error rate that is related to the normal images which is predicted cancer incorrectly is major drawback of thermography images, and attention to reduce of FP error rate has been insignificant in the previous works.

Our aim in this paper is to use asymmetry analysis for detecting the healthy and cancerous breasts from thermography images and also to reduce FP error rate by means of decision-level fusion. For this purpose, we define a novel texture feature based on Markov Random Field (MRF) model that is called MRF-based probable texture feature. In this feature, two modified versions of Local Binary Pattern (LBP) are applied to choose effective and appropriate cliques in the MRF model. Also, we introduce difference between co-occurrence levels (DCL) as a novel potential function in the MRF model for probable feature extraction. Also, to determine the cancerous cases from normal cases, a classification contemporary with decision level fusion by means of Hidden Markov Model (HMM)

is employed to fuse different extracted features from an image. This decision framework has been designed to reduce the FP error rate.

The rest of this paper is organized as follows. Section 2 explains the principles of our proposed breast cancer detection structure in details. The experimental results of our proposed breast cancer detection and also conclusion are provided in sections 3 and 4, respectively.

2. Proposed Breast Cancer Detection Structure

A DITI of a breast cancer patient and a healthy breast along with their temperature maps are shown in Fig. (1-a) and Fig. (1-b). Increasing the cellular consecutive dividing in the cancer cells makes the increase of metabolism and temperature in these cells and surrounding areas. These regions are seen as red spots in the DITI. Gray scale thermography imaging is applied in our proposed structure. Thus, all of images are converted from color format into gray scale by following equation [25].

$$grayscale = 0.21R + 0.71G + 0.07B \quad (1)$$

where R, G and B are the red, green and blue bands of color image, respectively.

The block diagram of proposed breast cancer detection structure is shown in Fig. 2. The first step in our proposed structure is the segmentation of the breast in the gray scale thermography images. The breast segmentation is performed through a simple masking method. Since, our proposed structure is based on asymmetric analysis; a method with minimal error in the segmentation is desired. Therefore, it is performed based on ROI cropping with a unit mask [15, 26, 27].

Note that all images have been resized to the same size before segmentation. The left and right breast segmentation of a gray scale thermograph is displayed in Fig. (3-a) and Fig. (3-b). All breast images have the similar sizes (300×400) after segmentation. In following, the feature extraction from each segmented breast including of proposed MRF-based probable texture feature and other texture features and also proposed two-stage decision structure including of asymmetric analysis and fusion-based classification using HMM will be described in details.

2.1. Feature Extraction

Asymmetric analysis is a popular method for detecting pathological cases in medical imaging particularly breast imaging. In this technique, the left and right breasts of each patient are compared with each other [7, 8, 15]. If asymmetry between the left and right breasts in each patient is more than a specified threshold, this will increase the probability of a cancer case in that patient. This analysis is rational due to in the most of patients; cancer starts from a breast and permeates to another breast and other region of the patient's body. Also, cancer incidence in both breasts simultaneously is extremely scarce [28]. Therefore, the use of asymmetric analysis method is permitted [8, 15, 26]. A point that must be considered to get acceptable results with this method is effective features extraction. In this paper, two sets of features are extracted based on MRF and modified LBP from the images that are described in detail in following.

2.1.1. MRF-based Probable Texture Feature Extraction

X_n is a Markov random process if its different conditions confirm Markov chain and satisfy the following equation:

$$P(X_n = x_n \mid X_k = x_k, k \neq n) = P(X_n = x_n \mid X_{n-1} = x_{n-1}, X_{n+1} = x_{n+1}) \quad (2)$$

The above equation implies that each element is related only to its neighbors and any changes in the non-neighboring elements does not have any influence on that element. Markov chains that are extended to multiple dimensions are called MRF. MRF is a statistical model that has been useful in several areas of image processing such as segmentation, texture perception and classification, image restoration and compression [29-32]. The use of Markov model in the above applications has three important steps as follows: 1) Define neighborhood system and clique; 2) Determine potential function; and 3) Define minimum or maximum energy changes as a decision criterion. For example in [29], each pixel will be in mass segment if its neighbors belong to mass. Thus, the criterion for mass segmentation in the breast is to minimize energy changes or maximize similarity measure.

Note that in the previous works, MRF model was employed in the segmentation, classification or even restoration of breast images [30-32]. While, we have proposed a novel texture feature that is extracted based on the MRF model. Definitely, feature extraction by means of MRF model is different in comparison with the other applications of MRF as mentioned in the above. The block diagram of our proposed algorithm for MRF-based probable texture feature extraction is shown in Fig. 2.

The coordinates of each pixel in an image is called "site" and these sites are associated with each other and define a neighborhood. A neighborhood system for "S" set is defined as follows:

$$N = \{N_i \perp \forall i \in s\} \qquad i \notin N_i \qquad i \in N_j \Leftrightarrow j \in N_i \tag{3}$$

where N_i is a set of adjacent sites, neighborhood relationship is mutual and a site is not consisting of its neighbors. In addition, a subset of the image sites makes a clique that each two cliques to be neighbors with each other.

2.1.1.1. Our Proposed Neighborhood System and Clique

Our images consist of 1,080,000 sites. These are divided into 120,000 blocks in our proposed MRF-based probable texture feature extraction algorithm. Each block is a (3×3) matrix whereby its center pixel is defined as $m_{i,j}$ and other pixels are the eight neighboring ones. Two features are extracted from each block as cliques. In fact, in our algorithm, instead of selecting a subset of sites, two features are extracted from each block as cliques and stored in two matrixes that are called CM1 and CM2 clique matrixes. The extracted features from each clique instead of a subset of neighboring sites have two major advantages: Firstly, two values (two features) are extracted from each 9 pixels to reduce computational complexity. Secondly, always there is a level of noise in the images. Therefore, the use of these pixels (9 pixels in the neighborhood) may lead to the wrong decision about the whole neighborhood. Since, in our proposed neighborhood system, the clique selection is performed with the feature extraction from each neighborhood and all pixels in a

neighborhood have influence on this selection, as a result, this decreases the wrong decision making for a clique.

In our algorithm, two different features are extracted from one block; thereby a similar arrangement is necessary to enumerate the image blocks. The enumeration is performed from left to right of each row and from the first to end row of the image. The arrangement of block is displayed in Fig. 4. The size of CM1 and CM2 matrixes are (300×400) and these two matrixes are replaced instead of the image matrix. In the next section, we describe our proposed neighborhood system and clique in detail.

2.1.1.1.1. Clique Matrix Definition Based on Modified LBP

Local Binary Pattern (LBP) is one of the popular techniques used for image representation and image texture classification [33]. LBP operator combines the characteristics of statistical and structural texture analysis that was first proposed by Ojala et al. [34]. LBP operator begins to act with specifying a neighborhood for each pixel and determining the center pixel as index in each neighborhood. Binary label for each pixel that can be either 0 or 1 as follows:

$$LBP_{P,R} = \sum_{P=0}^{P-1} s(g_p - g_c)2^P \qquad S(X) = \begin{cases} 1 & X \geq 0 \\ 0 & X < 0 \end{cases} \tag{4}$$

LBP operator obtains texture feature through the sum of weighted codes. Thus, reading from left or right of binary codes in each neighborhood is significant [35]. In our algorithm, like Ojala method, LBP code for each neighborhood is achieved based on equation (4). However, in our proposed algorithm, two different features are extracted from each LBP code with a novel strategy. The first feature is related to the low frequency (intensity) information of the image that is called Local Binary Pattern-color (LBPc) and the second feature is related to the high frequency (edge) information of the image that is called Local Binary Pattern-edge (LBPe). The extracted LBPc features are stored in CM1 matrix (the first clique matrix) and the extracted LBPe features are stored on CM2 matrix (the second clique matrix). Therefore, two features are extracted from each

binary pattern in the neighborhood, instead of converting it to the decimal number. Reading LBPc codes from left or right in each neighborhood is not significant and this issue is also true in the majority of LBPe codes. The center pixel of each neighborhood ($m_{i,j}$) and its eight neighbors is shown in Fig. 5. LBPc is calculated by the sum of bits in each binary pattern as follow,

$$LBPc = \left(\sum_{l=-1}^{1} \sum_{k=-1}^{1} m_{(i-1,j-k)} \right) - m_{i,j} \tag{5}$$

where $m_{i,j}$ is the center pixel of neighborhood. Thus, there are nine color levels [0-8]. In this feature, the difference of gray levels between center pixel and its neighborhood is considered as distinguishing information. For instance, color level in two patterns (11110000, 10101010) and one pattern (11111000) are four and five, respectively. Therefore, LBPc is focused on color feature of a block and implies to color level of pixels in blocks.

In the LBPe feature, the alteration between bits in each binary code is considered as an important feature. As previously mentioned, two patterns (11110000, 10101010) have similar LBPc feature. To distinguish these two different patterns, we define the LBPe feature. This feature is extracted based on any changes from 0 to 1 in each pattern. Thus, the change levels can vary in the range [0-7]. For example, pattern "10101010" has seven change levels but patterns "11111111" or "00000000" have zero change level. The LBPe feature is defined as following:

$$LBPe = \sum_{i=1}^{7} \left| u(i+1) - u(i) \right| \tag{6}$$

where u is a vector that is defined based on introduced neighborhood in Fig. 5, as,

$$\mathbf{u} = [\mathbf{m_{i-1,j-1}}, \mathbf{m_{i,j-1}}, \mathbf{m_{i+1,j-1}}, \mathbf{m_{i+1,j}}, \mathbf{m_{i+1,j+1}}, \mathbf{m_{i,j+1}}, \mathbf{m_{i-1,j+1}}, \mathbf{m_{i-1,j}}] \tag{7}$$

Indeed, non-homogeneity of the pixels in a block is specified by LBPe. Therefore, LBPe has a higher value in the blocks that are related to different parts of image with intense edges. While, the blocks associated to the homogeneous areas of image have lower values of LBPe. Because, there are similar textures, fewer changes, and little edges in the image homogeneous regions. Thus, color

and edge levels related to each block of image are stored in the CM1 and CM2. An example of LBPc and LBPe calculation are displayed in Fig. 6.

2.1.1.2. Potential Function Definition

Selection of an appropriate potential function is crucial, when the MRF model is used as a tool in the image processing application. According to MRF model, the energy of each clique should be determined and each clique belongs to a class which its relevant energy is the minimum value.

In our algorithm, it is not essential to compute the value of energy in each clique and compare them with other classes. Our aim is to determine the rate of energy alterations between cliques as a feature that extracted from left and right breasts. The more changes in the cliques indicate that breast texture is non homogeneous and breast texture have different segments and numerous edges. Therefore, these are considered to be abnormal breast specifications. In contrast, if the changes between cliques are low, i.e. the most of cliques have similar features in terms of edge. This issue represents a breast with uniform texture without edges (normal breast). Therefore, the aim is not to identify the breast lump but our goal is to extract those features able to express lump probability by a proper way. Thus, energy function is beneficial since it is able to identify the changes between cliques even too low. In this paper, we apply three different energy functions which can be considered more attention to the relationship between cliques and their relevant alterations in order to calculate the energy changes.

2.1.1.2.1. First Proposed Potential Function - Entropy

In some of the related works, Shannon entropy, mutual Information, and also different similarity measures have been used as the energy functions for segmentation or classification based upon MRF model [36]. Thus, we have used Tsallis entropy to extract the rate of energy changes between cliques in each CM1 and CM2 matrixes. In previous works, Shannon entropy has been effective for the identification of irregularity and chaos in the different models. However, in some applications

such as our application in which even little changes cannot be avoided, Shannon entropy is unsuccessful. The Tsallis and Shannon entropies are defined as:

$$Tsallisentropy = \frac{1-\sum p_i^q}{1-q} \quad (8)$$

$$shannonentropy = \sum -p_i \log p_i \quad (9)$$

where p_i probability density function and q is a parameter that is selected based on the application. The "q" parameter in Tsallis entropy is helpful like an adaptive filter such a way that we will be able to identify even low changes in each matrix by the appropriate selection of q. Note that before computing entropy in each CM1 and CM2 matrix, these matrixes become the same scale in range [0,1]. Thus, energy changes between entries of clique matrixes are computed by Tsallis entropy. Euclidean distance measure is used to compare the energy changes between entries of clique matrixes of left and right breasts. Our first feature that is called TLBPc created from the comparison of energy changes between the CM1 matrix of left and right breasts in each image. In addition, if we compare those changes calculated by means of Tsallis entropy in the CM2 matrix of left and right breasts, the second feature is obtained that is named TLBPe.

2.1.1.2.2. Second Proposed Potential Function - GLCM

As indicated before, the CM1 and CM2 matrixes are composed of real numbers from 0 to 8 and 0 to 7, respectively. With regard to small values of clique matrix elements, proper potential function should be selected that can be extracted little changes occurred between cliques. Since, the operators can be useful that are able to specify the relationship between pixels precisely. Thus, we use the gray level co occurrence matrix (GLCM) as the second potential function.

GLCM represents the second order statistics based on neighboring pixels and it is a two dimensional array, which takes into account the specific position of a pixel relative to the other pixels. The GLCM is a tabulation of different combination of pixel brightness values occur in an image. This matrix with (8×8) elements is constructed at a distance of $d=1$ for various directions

given as $0°,45°,90°,180°$ [37]. In normal applications, the GLCM is used for feature extraction from image texture, while it has been used as an energy function in our application. By using GLCM, we are able to obtain the amount of changes occurred between pixels of CM1 and CM2 matrixes. We apply GLCM in four directions and $d=1$. Therefore, four (8×8) matrixes are obtained for each clique matrix and considered as a potential function. Ultimately, two new GLBPc and GLBPe features are obtained from the comparison of energy changes in the CM1 and CM2 matrixes that these energy changes are calculated by GLCM in the left and right breasts.

2.1.1.2.3. Third Proposed Potential Function – DCL

DCL vector is defined as third potential function that is formed from GLCM based on a novel scenario. In fact, this novel energy function obtained from the difference between co-occurrence levels (DCL) in the GLCM matrix. The DCL vector has more attention towards the brightness level value between a pixel and its neighbors. In DCL, the value of pixel and its neighbors is not important, but difference values in the pixel brightness level with its neighbors is crucial. The first element of DCL vector is generated from the sum of all GLCM matrix entries, which their subtraction of row (i) and column (j) equals to 1. The second element is derived from total GLCM matrix entries, which the difference between i and j values is equal to 2. This method will continue to produce the seventh element of DCL vector. The DCL vector is formed as

$$DCL(k)=\sum_{i,j} GLCM(i.j), \quad if \quad |i-j|=k \; and \; k=1,2,..7 \tag{10}$$

where GLCM is the co-occurrence matrix with 8 levels. In fact, DCL vector is created based on the rate of difference between the rows and columns of GLCM. Both DCL and GLCM are able to determine the changes occurred between cliques of an image. The process of DCL vector extraction from GLCM matrix is shown in Fig. 7. Two new DLBPc and DLBPe features are defined by applying the DCL as energy function in the CM1 and CM2 matrixes.

2.1.2. Texture Feature Extraction

LBP is a popular technique used for image representation, classification and feature extraction. The modified LBP that we introduced in section (2.1.1.1.1) to select appropriate cliques in the MRF model; can extract valuable information from the texture feature of the images. Therefore, we use the LBPe and LBPc as tools for extraction of edge and intensity features. For this purpose, Euclidean distance of LBPc and LBPe histograms of left and right breasts are introduced as HLBPc and HLBPe texture features. Also, the sum of LBPe and LBPc codes in left and right breasts are called LBPcs and LBPes. Euclidean distance of LBPcs and LBPes of left and right breasts are used as two other effective features.

Since, GLCM is a useful tool for texture feature extraction from the images. Therefore, we extract another texture feature from the left and right breasts based on GLCM. For this purpose, our last proposed texture feature is introduced based on comparison of GLCM matrixes of left and right breasts. This feature that is called Difference of GLCM Matrixes (DGM) is defined by sum of Euclidean distance of corresponding GLCM matrixes of left and right breasts in four directions.

2.2. Primitive Decision Based on Asymmetric Analysis

Normal images can be separated from the abnormal ones by means of any one of the aforesaid features individually and a simple classifier like a linear decision boundary. In order to choose a linear decision boundary in each feature, initially images are divided to test and train datasets. A decision boundary in each feature is selected based on images of training dataset by means of Leave-One-Out (LOO) cross-validation strategy. Using the decision boundary selection for each feature, the success rate and also error rate of each feature in the normal and cancer breast classification are specified. It means that we have identified the number of normal cases detected as normal (TN) as well as the number of cases predicted as the cancer (FP) wrongly and also the number of cancer cases diagnosed as cancer (TP) or normal cases incorrectly (FN). As regards 11 features are extracted from each image, thus 11 primitive decisions are obtained for each image.

Certainly, the accuracy rate and FP error rate of breast cancer classification by each feature individually are not appropriate. Therefore, we should apply a further process for improving the classification results.

2.3. Decision-level Fusion-based Classification using HMM

However, our aim is to improve classification accuracy using decision level fusion so that the results of all features can be used for an image simultaneously. In our algorithm, a general decision will be achieved for an image by fusing the 11 primitive decisions that are mentioned in section (2.2). Thus, there are sequences of observation for each image and our aim is to determine the best decision for each image based on its observation. Since, we propose HMM as a tool that is able to merge different features and adopt the best decision for each image.

Each HMM is defined by states, state probabilities, transition probabilities, emission probabilities and initial probabilities [38-39]. The N states of model and also M observation symbols per state are defined by $s = \{s_1, s_2, ..., s_N\}$ and $V = \{v_1, v_2, ..., v_M\}$, respectively. If the observations are continuous then M is infinite.

The state transition probability distribution $A = \{a_{ij}\}$, where a_{ij} the probability that the state at time $t+1$ is s_j, is given when the state at time t is s_i. The structure of this stochastic matrix defines the connection structure of the model. If a coefficient a_{ij} is zero, it will remain zero even through the training process, so there will never be a transition from state s_i to s_j.

$$a_{ij} = p\{q_{t+1} = j | q_t = i\} \quad , \qquad 1 \le i, j \le N \tag{11}$$

where q_t denotes the current state. The transition probabilities should satisfy the normal stochastic constraints,

$$a_{ij} \ge 0, \quad 1 \le i, j \le N, \quad \sum_{j=1}^{N} a_{ij} = 1 \quad , \qquad 1 \le i \le N \tag{12}$$

The observation symbol probability distribution in each state, $B = \{b_j(k)\}$ where $b_j(k)$ is the probability that symbol v_k is emitted in state s_j.

$$b_j(k) = p\{o_t = v_k \mid q_t = j\} \qquad 1 \le j \le N, 1 \le k \le M \tag{13}$$

where v_k denotes the k^{th} observation symbol in the alphabet, and o_t the current parameter vector. The following stochastic constraints must be satisfied:

$$b_j(k) \ge 0, \qquad 1 \le j \le N, \quad 1 \le k \le M, \qquad \sum_{k=1}^{M} b_{j(k)} = 1, \quad 1 \le j \le N \tag{14}$$

And finally the initial state distribution π that is related to state in time $t = 0$ [39].

The cancer and normal are two states and 11 extracted features are the possible observations in our HMM model. As previously mentioned, there is a decision boundary for each feature or observation. Thus, 11 possible observations are characterized for each image that can be larger or smaller from their corresponding decision boundaries. For this purpose, there are other hidden observations in each observation in our model. The observations which the numerical values are greater than their corresponding decision boundaries are called “main observations”. In contrast, hidden observations are smaller than their decision boundaries. The diagram of our HMM model is shown in Fig. 8. In this diagram, 11 main and hidden observations are shown by solid and dotted ellipses, respectively. Therefore, each image has its own unique model in terms of observation type. In fact, based on the extracted features of each image, the type of observations and model of image are determined.

The operation of our proposed HMM model for classification contemporary with decision-level fusion is generally similar to other hierarchical decision structures such as decision tree, random forest and also other methods that perform the fusion in the feature or decision level [40-43]. But, they have the differences together in details and application. Generally, the decision tree is beneficial when some features have more accurate predictions than to other features. Also, the random forest selects a random subset of input features to construct each decision tree. However, this method is unable to achieve our aim due to choose the number of features to construct decision

tree. While, in our model, all features intervene to decision and the classification is performed in a parallel state and simultaneously. While, the classification based on random forest and decision tree is carried out hierarchically and the features are used to decide in different steps of the tree [42-43].

2.3.1. Transition Matrix Definition in our HMM model

As previously mentioned the cancer and normal are two states and 11 extracted features are the possible observations in our application. As regards, cancer or normal diagnosis for an image should not have any effect on the previous or next image that is going to be evaluated. The state transition probabilities for both cancer and normal states are equal to 0.5. Therefore, transition matrix is defined as follows:

$$A = \begin{bmatrix} 0.5 & 0.5 \\ 0.5 & 0.5 \end{bmatrix} \tag{15}$$

2.3.2. Emission Probabilities in our HMM Model

The main stage of decision-level fusion is performed based on emission probability matrixes in our proposed HMM model. As regards, there are two different types of observation in our HMM model. Therefore, two emission probability matrixes are considered.

The rate of TP determines the output probability of cancer state to main observations and output probability from cancer state to hidden observations are specified by the rate of FP in each feature. In addition, output probability of normal state to main observations is obtained by the rate of FN and to hidden observations is determined with the rate of TN (Fig. 8). Output probabilities of both states to main observations are shown in B_m matrix which the first row is related to cancer state and the second one is concerned to the normal state as follow:

$$\mathbf{B_m} = \begin{bmatrix} b_{m11} b_{m12} b_{m13} \ldots b_{m1n} \\ b_{m21} b_{m22} b_{m23} \ldots b_{m2n} \end{bmatrix} \tag{16}$$

The emission probabilities of normal and cancer states to hidden observations are displayed in B_h matrix and its first and second rows are related to the cancer and normal, respectively, as follow:

$$\mathbf{B_h} = \begin{bmatrix} b_{h11} b_{h12} b_{h13} \dots b_{h1n} \\ b_{h21} b_{h22} b_{h23} \dots b_{h2n} \end{bmatrix} \quad (17)$$

Note that the output probabilities are obtained based on experimental results on the training dataset. Thus, there is an observation sequence and output probability for each image and our aim is to choose the optimal state or best decision for an image.

2.3.3. Final Decision Determination

Our goal is to determine the class of each image based on observation sequence and its output probabilities. Thus, we should calculate dependency probability of each image to cancer or normal class individually. This means that two conditional probabilities $P(c|I)$ and $P(n|I)$ are computed for image I. If $P(c|I)$ for image I is more than $P(n|I)$, then our image will be a cancer case. In contrast, if $P(n|I)$ is greater than $P(c|I)$, then image will be a normal case. The classification of image I in mathematical terms is carried out as follows:

$$I = \begin{cases} Normal & P(c|I) < P(n|I) \\ Cancer & P(c|I) \geq P(n|I) \end{cases}, \quad \begin{matrix} 0 \leq P(c|I) \leq 1 \\ 0 \leq P(n|I) \leq 1 \end{matrix} \quad (18)$$

After determining the number of main (m) or hidden (h) of observations, we will characterize their corresponding output probabilities. $P(c|I)$ and $P(n|I)$ are computed by taking the average of output probabilities for the normal and cancer states. In fact, $P(c|I)$ is calculated by average of b_j for the cancer state, and $P(n|I)$ is obtained by taking the average of b_j for the normal state. Therefore, $P(c|I)$ and $P(n|I)$ are defined as below:

$$P(c|I) = \frac{\sum_{k=1}^{N} B_j(1,k)}{N} \quad (19)$$

$$P(n \mid I) = \frac{\sum_{k=1}^{N} B_j(2,k)}{N} \quad (20)$$

where N is the number of extracted features ($N = 11$) and B_j ($j \in \{m, h\}$) are the emission probabilities of normal and cancer states to the main and hidden observations.

3. Experimental Results

We have studied 65 breast thermography images available and obtained from [20, 21, 24]. Although the images from these sources are varied in their resolutions and generally did not follow a unified protocol, our algorithm could separate cancer cases from normal ones without any problem. Our database is divided into training dataset consisting of 33 images and test dataset consisting of 32 images for training (parameter tuning) and evaluation of our proposed structure.

3.1. MRF-based Probable Texture Feature Extraction

To determine clique in our proposed MRF-based probable texture feature, the image is divided into (3×3) blocks so that two features were extracted from each block. Then, each extracted feature makes a clique matrix. Feature extraction from each neighborhood instead of choosing a subset of sites as clique is led to improve the classification performance. The size of blocks can be changed based on desirable sensitivity of feature extraction process. Two different sizes of blocks have been implemented in our database images. The rate of FP will be reduced if the images are divided into (5×5) blocks. In fact, with increasing the block size, small changes of edge or color in the images are affected on the extracted features. In other words, with large blocks, the TN will be correctly diagnosed in some normal images that have small differences between their left and right breasts, while these images are predicted FP incorrectly with (3×3) blocks. However, (5×5) blocks are led to incorrectly diagnosis in some images related to situ or localized cancer or cancer in the early stage. As regards, wrong diagnosis of FN is irreparable. Therefore, the (3×3) blocks are used in our application. As, the blocks have not any overlap, computational complexity of our algorithm is

low, while feature extraction from blocks with overlapping causes increasing the computational complexity severely. Since, the improvement of performance is too small by utilizing overlap blocks. Thus, the images are divided into (3×3) blocks without any overlap.

3.2. Primitive Decision Results

Leave-One-Out (LOO) cross-validation is an evaluation scheme repeatedly which trains an algorithm on the full dataset excluding only one example and then performs test on it. In our primitive decision algorithm, to select the decision boundary of each feature, LOO is applied on the 35 images of training dataset. The feature mean of these images is considered as primitive decision boundary for each feature. The success rate of classification by means of each feature and the corresponding decision boundary on the test and training images is obtained in Table 1. In this table, the first six features (column F1 through column F6) are the MRF-based probable texture features that defined based on three different potential functions in our MRF. The columns F7 until F11 indicate the other texture features that described in section (2.1.2). The number of TN, TP, FN and FP are displayed in this table. Also the total of FP and FN (i.e. total of errors (TOE)) is specified in Table 1.

In our MRF-based probable texture feature, Shannon entropy was used as potential function in the CM1 and CM2 matrixes but this entropy had no significant result. But, Tsallis entropy obtains better performance when is used as potential function in the MRF. The parameter q in the Tsallis entropy is success reason of Tsallis entropy relative to Shannon entropy. Both Tsallis and Shannon entropies can extract chaos and change of image. However, the parameter q in the Tsallis entropy is like a filter that can extract the small changes from image by selecting a proper value for q. In the Tsallis entropy $q=2$ has the best performance in the training dataset while with increment or reduction of parameter q, the number of errors is increased in TLBPc and TLBPe features.

3.3. Detection Results by Our HMM Classifier

To detect the breast cancer by our proposed fusion-based classifier, the introduced emission matrixes (B_m and B_h) in our HMM model in section (2.3.2) should be determined. For this purpose, we compute the elements of B_m and B_h matrixes based on training images. The first and second rows of B_m matrix are related to the output probabilities of cancer and normal states to the main observation, respectively. The first and second rows of B_h matrix are related to the output probabilities from cancer and normal states to the hidden observation, respectively. The rate of TP in the training dataset determines the output probability of cancer state to main observations and the output probability from cancer state to hidden observations are specified by the rate of FP in each feature. In addition, the output probabilities of normal state to the main and hidden observations are obtained by the rate of FN and TN, respectively. Therefore, the effectiveness of each feature is specified in B_m and B_h matrices. The obtained B_m and B_h matrixes from our training dataset are as following:

$$\mathbf{B_m} = \begin{bmatrix} \mathbf{0.8\ 0.75\ 0.75\ 0.7\ 0.8\ 0.65\ 0.9\ 0.75\ 0.85\ 0.8\ 0.8} \\ \mathbf{0.2\ \ .25\ \ 0.25\ 0.3\ 0.2\ 0.35\ 0.1\ 0.25\ 0.15\ 0.2\ 0.2} \end{bmatrix} \quad (21)$$

$$\mathbf{B_h} = \begin{bmatrix} \mathbf{0.31\ 0.08\ 0.08\ 0.08\ 0.24\ 0.23\ 0.31\ 0.15\ 0.23\ 0.15\ 0.31} \\ \mathbf{0.69\ 0.92\ 0.92\ 0.92\ 0.76\ 0.77\ 0.69\ 0.85\ 0.77\ 0.85\ 0.69} \end{bmatrix} \quad (22)$$

It is obvious that almost all features have the same performance and efficiency approximately and our aim is the decision based on all features simultaneously.

To evaluate our algorithm perfectly, we use some criteria such as Positive Predictive Value (PPV), Negative Predictive Value (NPV), Sensitivity (SEN) and Specificity (SPC) that are defined as following,

$$PPV = \frac{TP}{TP + FP} \quad (23)$$

$$NPV = \frac{TN}{TN + FN} \quad (24)$$

$$SEN = \frac{TP}{TP + FN} \quad (25)$$

$$SPC = \frac{TN}{FP + TN} \quad (26)$$

Table 2 obtains the fusion results of our breast cancer detection algorithm based on TP, TN, FP, TOE, PPV, NPV, SEN and SPC measures. According to Table 1, the least value of TOE for all features is four samples on the test dataset. By our decision-level fusion algorithm, the numbers of errors are reduced to two samples in our test dataset (Table 2). Also, Receiver Operating Characteristic (ROC) curve on the test and training datasets is shown in Fig. 9.

Thermography image related to an FP case is shown in Fig. 10. This normal image has some segments with red color and sometimes pulmonary and respiratory problems or vascular pattern of the patient's body are the reasons of the aforesaid red segments in the thermography images. The features that are extracted from color pixels of the images such as TLBPc, LBPcs, and GLBPc determine cancer class for this normal image, while this image is belonging for the normal class. Note that TLBPe and LBPes are diagnosed as normal for this image in a correct way. Therefore, it is essential to use different features simultaneously in order to improve the classification results.

Table 3 obtains the middle results of our breast cancer detection algorithm for six selected samples from our dataset. The "h" and "m" are related to the hidden and main observations and probability of cancer and normal states are available in the B_h and B_m matrixes. All observations in the first row are "h". It means that all features have acted correctly for this normal case. The value of energy changes must be less than decision boundaries for the normal cases. In other words, each observation has to be hidden for the normal cases if the feature related to its observation has been effective to this normal case. It is expected that the value of energy changes in each feature is greater than its decision boundary in the cancer cases. Therefore, if one feature is effective in the cancerous images, then its corresponding observation will be the main observation. The third and fourth rows of Table 3 refer to a cancerous and a normal sample. Although, the features F5 and F6 have operated incorrectly for the third and fourth images, respectively. But, the final detection has

carried out correctly by using our decision-level fusion algorithm. The last two rows of Table 3 are related to an FP and an FN case. Since; the most features have been detected incorrectly. The final decisions made by our decision-level fusion algorithm also are incorrectly. Finally, with applying our decision-level fusion algorithm on the images of dataset, only 8 images of 65 images were not detected correctly and other images were assigned to true classes.

4. CONCLUSION

In our proposed breast cancer detection algorithm, normal and abnormal patterns were separated from each other through texture features that were defined for first time in this work. In this paper, we analyzed thermal breast images using MRF-based probable texture and LBP features to determine difference between the normal and abnormal cases. The results of this study indicated that useful features of texture can be extracted with MRF models, LBPc and LBPe. In addition, with asymmetric analysis and comparison of effective features from left and right breasts, the breast cancer was detected by our proposed decision-level fusion HMM-based algorithm.

Acknowledgement

The authors would like to sincerely thank the anonymous referees for their useful comments which help us to improve the paper.

References

[1] A. Jemal, R. Siegel, E. Ward, Y. Hao, J. Xu, M. J. Thun, "Cancer statistics," CA: A Cancer Journal for Clinicians, Vol. 60, No. 5, pp. 277-300, Sep 2010.

[2] J. Head, F. Wang, C. Lipari, R. Elliott, "The Important Role of Infrared Imaging in Breast Cancer," IEEE Engineering in Medicine and Biology, Vol. 19, pp. 52-57, 2000.

[3] Y. R. Parisky, A. Sardi, R. Hamm, K. Hughes, L. Esserman, S. Rust, K. Callahan, "Efficacy of Computerized Infrared Imaging Analysis to Evaluate Mammographically Suspicious Lesions," American Journal of Roentgenology, Vol. 180, No. 1, pp. 263-269, January 2003.

[4] D. Kennedy, T. Lee, D. Seely, "A Comparative Review of Thermography as a Breast Screening Technique," Integrative Cancer Therapies, vol. 08, pp. 9-16, 2009.

[5] B. F. Jones, "A reappraisal of the use of infrared thermal image analysis in medicine," IEEE Transactions on Medical Imaging, Vol. 17, No, 6, pp. 1019-1027, 1998.

[6] E. Y. K. Ng, L. N. Ung, F. C. Ng, L. S. J. Sim, "Statistical analysis of healthy and malignant breast thermography," Journal of Medical Engineering and Technology, Vol. 25, pp. 253-263, 2001.

[7] H. Yang, SH. Xie, Q. Lin, SH. Ye, SH. Chen, H. Li, "A new infrared thermal imaging and its preliminary investigation of Breast Disease Assessment," Proc. of IEEE/ICME, International Conference on Complex Medical Engineering, pp. 1071-1074, 2007.

[8] H. Qi, W. Snyder, J.F. Head, R.L. Elliott, "Detecting breast cancer from infrared images by asymmetry analysis," Proc. 22nd Annu. Conf. IEEE Engineering in Medicine and Biology Society, Chicago, pp. 23–28, July 2000.

[9] M. Frize, C. Herry, R. Roberge, "Processing of thermal images to detect breast cancer," 4th International IEEE EMBS Special Topic Conference on Information Technology Applications in Biomedicine, Vol. 680, pp. 234-237, 2003.

[10] X. Tang, H. Ding, Y. Yuan, Q. Wang, "Morphological Measurement of Localized temperature Increase Amplitudes in breast Thermograms and its clinical application", Biomedical Signal processing and Control, Vol 3, pp 312-318, 2008.

[11] P. Kapoor, E**.** Bhayana, "Real Time Intelligent Thermal Analysis Approach for Early Diagnosis of Breast Cancer", International Journal of Computer Applications, Vol. 1, No.5, pp 22-24, 2010**.**

[12] H. Ghayoumi Zadeh, A. Kazerouni, Haddadin, "Distinguish breast cancer based on thermal Features in Infrared Images," Canadian Journal on Image processing and computer vision, Vol. 2, pp. 54-58, 2011.

[13] H. Ghayoumi Zadeh, O. Pakdelazar, J. Haddadnia, Gh. Rezai-Rad, M. Mohammad-Zadeh, "Diagnosing Breast Cancer with the Aid of Fuzzy Logic Based on Data Mining of a Genetic Algorithm in Infrared Images," Middle East Journal of Cancer, Vol. 3, No. 4, pp. 119-129, 2011.

[14] O. D. Nurhayati, Th. Widodo, A. Susanto, M. Tjokronagoro, "First Order Statistical Feature for Breast Cancer Detection Using Thermal Images," World Academy of Science Engineering and Technology, Vol. 46, pp. 424-426, 2010.

[15] O. D. Nurhayati, A. Susanto, T. Sri Widodo, "Detection of the Breast Cancer from Thermal Infrared Images based on Statistical Characteristics," International Journal of Science Engineering and Technology, Vol. 2, No. 2, pp. 65-69, 2009.

[16] M. EtehadTavakol, S. Sadri, E.Y.K. Ng, "Application of K-means and fuzzy c-means for color segmentation of thermal infrared breast images", Journal of Medical Systems, Vol. 34, No.1, pp. 35–42, 2010.

[17] M. EtehadTavakol, E.Y.K. Ng, C. Lucas, S. Sadri, M. Ataei "Nonlinear analysis using Lyapunov exponents in breast thermograms to identify abnormal lesions," Infrared Physics & Technology, Vol. 55, pp. 345-352, 2010.

[18] Q. Huang, X. Bai, Y. Li, L. Jin, X. Li, "Optimized graph-based segmentation for ultrasound images", Neurocomputing, Vol.129, pp. 216-224, 2014.

[19] N. Selvarasu, Alamelu Nachiappan, N.M. Nandhitha, "Effective Representation of Non-Uniformity and Asymmetry in Breast Thermographs using Statistical Parameters on Histograms of Wavelet Coefficients for Cancer Detection," European Journal of Scientific Research, vol. 80, No. 1, pp. 10-19, 2012.

[20] M. Etehad Tavakol, C. Lucas, S. Sadri, E.Y.K. Ng, "Analysis of breast thermography using fractal dimension to establish possible difference between malignant and benign patterns," Journal of Health care Engineering, Vol. 1, No. 1, pp. 27–43, 2010.

[21] M. Etehad Tavakol, E.Y.K. Ng, C. Lucas, S. Sadri, N. Gheissari, "Estimating the mutual information between bilateral breast in thermograms using nonparametric windows, " Journal of Medical Systems, Vol. 35, No. 5, pp. 959-967, 2011.

[22] M. Wiecek, R. Strakowski, T. Jakubowska, B. Wiecek, "Software for classification of thermal imaging for medical applications," 9th International Conference on Quantitative Infrared Thermography, vol. 14, N0. 2, 2008.

[23] N. Selvarasu , "Image Processing Techniques and Neural Networks for Automated Cancer Analysis from Breast Thermographs-A Review," Indian Journal of Computer Science and Engineering (IJCSE), vol. 3, No. 1, pp. 133-137, 2012.

[24] R. Rastghalam, H. Pourghassem, "Breast Cancer Detection Using Spectral Probable Feature on Thermography Images," 8th Iranian Conference on Machine Vision and Image Processing (MVIP), pp. 802-806, September 2013.

[25] M. Nurmohamadi, H. Pourghassem, "Clavulanic acid production estimation based on color and structural features of streptomyces clavuligerus bacteria using self-organizing map and genetic algorithm", Computer Methods and Programs in Biomedicine, Vol. 114, No. 3, pp. 337-348, May 2014.

[26] G. Schaefer, M. Závišek, T. Nakashima, "Thermography based breast cancer analysis using statistical features and fuzzy classification", Pattern Recognition, Vol. 42, No. 6, PP. 1133-1137, June 2009.

[27] P. Kapoor, S. Prasad, S. Patni, "Image Segmentation and Asymmetry Analysis of Breast Thermograms for Tumor Detection", International Journal of Computer Applications, Vol. 50, No. 9. 2012.

[28] Sh. Babazadeh, A. Andalib, A. Amuheidari, "A Study of Long Term Trend for Breast Cancer Epidemiological Factors and Clinical Parameters in Isfahan Province", Journal of Isfahan Medical School, Vol. 29, No. 161 1st week, January 2012.

[29] A. Ashraf, S. Gavenonis, D. Daye, C. Mies, M. Rosen, D. Kontos, "A Multichannel Markov Random Field Framework for Tumor Segmentation With an Application to Classification of Gene Expression-Based Breast Cancer Recurrence Risk," IEEE Transactions on Medical Imaging , Vol. 32, No. 4, pp. 637-648, April 2013.

[30] H. D. Li, M. Kallergi, L.P. Clarke, V.K. Jain, R.A. Clark, "Markov random field for tumor detection in digital mammography", IEEE Transactions on Medical Imaging, Vol. 14, No. 3, pp. 565-576, 1995.

[31] R. Nishii, S. Eguchi, "Image classification based on Markov random field models with Jeffreys divergence", Journal of Multivariate Analysis, Vol. 97, No. 9, pp. 1997 – 2008, 2006.

[32] A. Ashraf, S.Gavenonis, D.Daye, C.Mies, M.Rosen, D.Kontos, "A Multichannel Markov Random Field Framework for Tumor Segmentation With an Application to Classification of Gene Expression-Based Breast Cancer Recurrence Risk", IEEE Transactions on Medical Imaging, Vol. 32, No. 4, pp. 637-648, April 2013.

[33] N. Jafari Fesharaki, H. Pourghassem, "Medical X-ray Image Hierarchical Classification Using a Merging and Splitting Scheme in Feature Space," Journal of Medical Signals and Sensors, Vol. 3, No. 3, pp. 150-163, 2013.

[34] T. Ojala, M. Pietikainen, T. Maenpaa, "Multiresolution gray-scale and rotation invariant texture classification with local binary patterns," IEEE Transactions Pattern Analysis and Machine Intelligence, vol. 24, No. 7, pp. 971–987, Jul. 2002.

[35] N. Abounasr, H. Pourghassem, "Facial Expression Recognition Using ALGBP-TOP", International Journal of Imaging and Robotics, Vol. 11, No. 3, pp. 11-23, Mar. 2013.

[36] Q. Razlighi, N. Kehtarnavaz, A. Nosratinia, "Computation of Image Spatial Entropy Using Quadrilateral Markov Random Field", IEEE Transactions on Image Processing, Vol. 18, No. 12, pp. 2629-2639, December 2009.

[37] H. Pourghassem, H. Ghassemian, "Content-based medical image classification using a new hierarchical merging scheme, " Computerized Medical Imaging and Graphics, Vol. 32, No. 8, PP. 651-661, December 2008.

[38] N. Nasehi, H. Pourghassem, "Mental Task Classification Based on HMM and BPNN," Communication Systems and Network Technologies (CSNT), pp. 210-214, April 2013.

[39] A. Tahmasebi, H. Pourghassem, "Signature Identification using Dynamic and HMM Features and KNN Classifier", International Conference on Communication Systems and Network Technologies (CSNT 2013), pp. 201-205, Gwalior, India, 6-8 Apr. 2013.

[40] X. Bai, E. R. Hancock, R. Wilson, "Graph characteristics from the heat kernel trace", Pattern Recognition, Vol. 42, No.11, pp. 2589-2606, 2009.

[41] X. Bai, Ch. Liu, P. Ren, J. Zhou, H. Zhao, Y. Su, "Object Classification via Feature Fusion Based Marginalized Kernels", IEEE Geosci Remote Sensing Lett, Vol. 12, No.1, pp. 8-12, 2015.

[42] V. Svetnik, A. Liaw, C. Tong, J. Culberson, R. Sheridan, B. Feuston, "Random forest: a classification and regression tool for compound classification and QSAR modeling", Journal of Chemical Information and Computer Sciences, Vol. 43, No. 6, pp. 1947-1958, November 2013.

[43] A. Heidema, N. Nagelkerke, "Developing a discrimination rule between breast cancer patients and controls using proteomics mass spectrometric data: a three-step approach", Statistical Applications in Genetics and Molecular Biology, Vol. 7, No, 2, pp. 1-11, Feb. 2008.

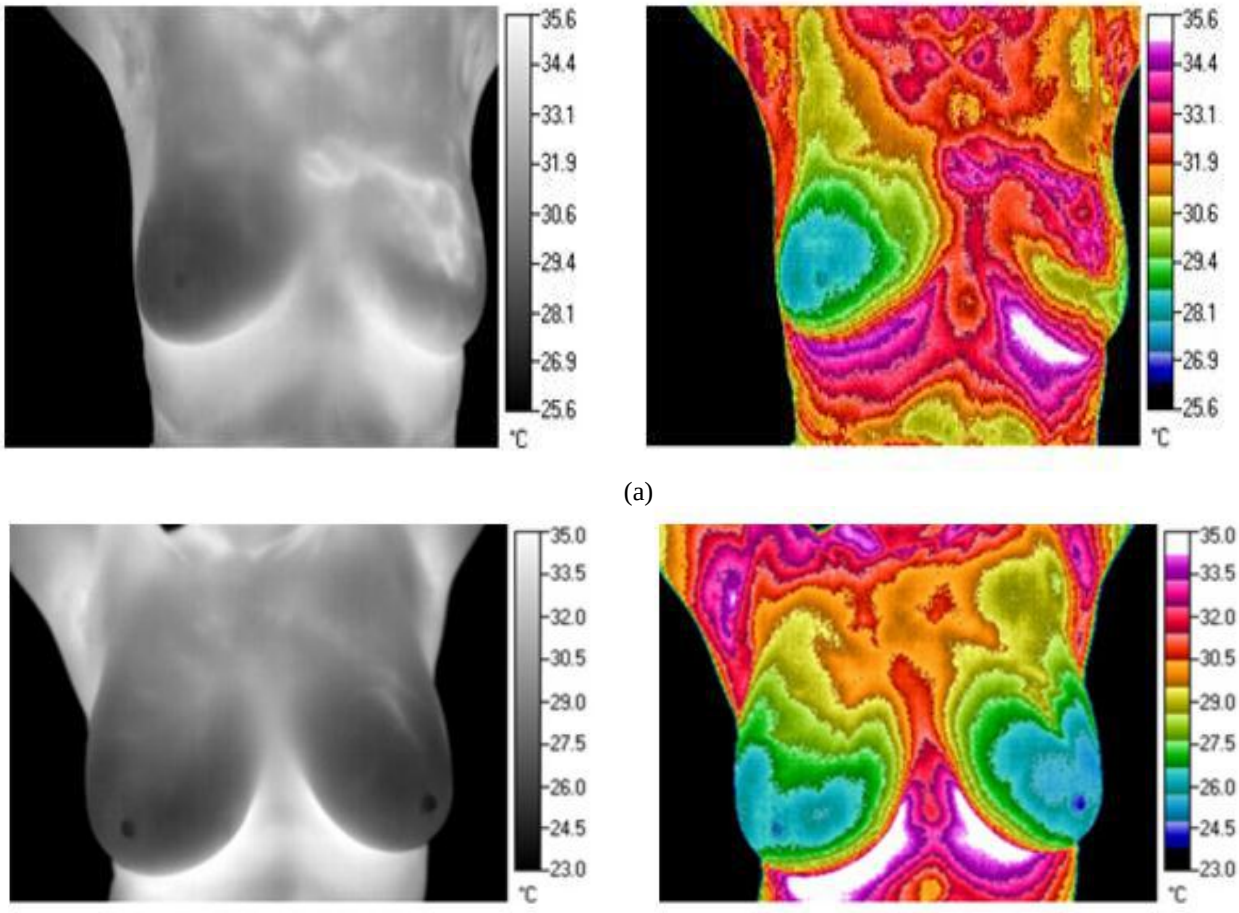

Fig. 1: Thermography images along with their temperature maps, (a) Cancerous case, (b) Normal case.

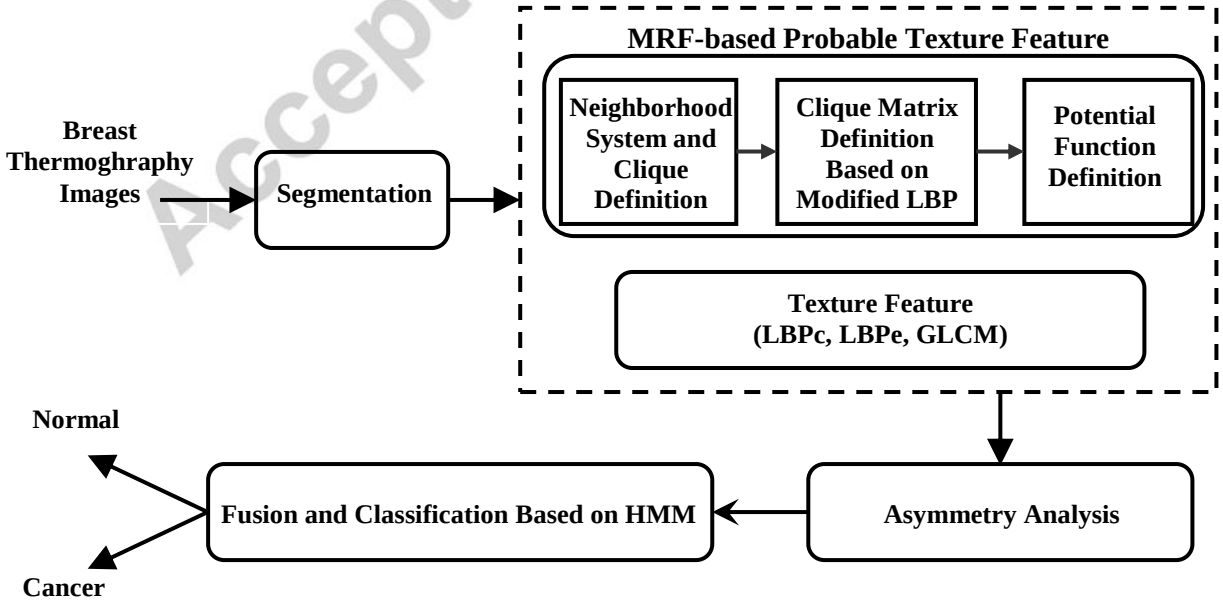

Fig. 2: Block diagram of the proposed breast cancer detection structure.

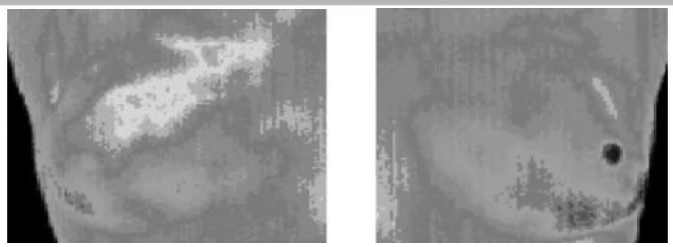

(a) **(b)**

Fig. 3: Breast segmentation, (a) and (b) left and right breast segments of an image sample.

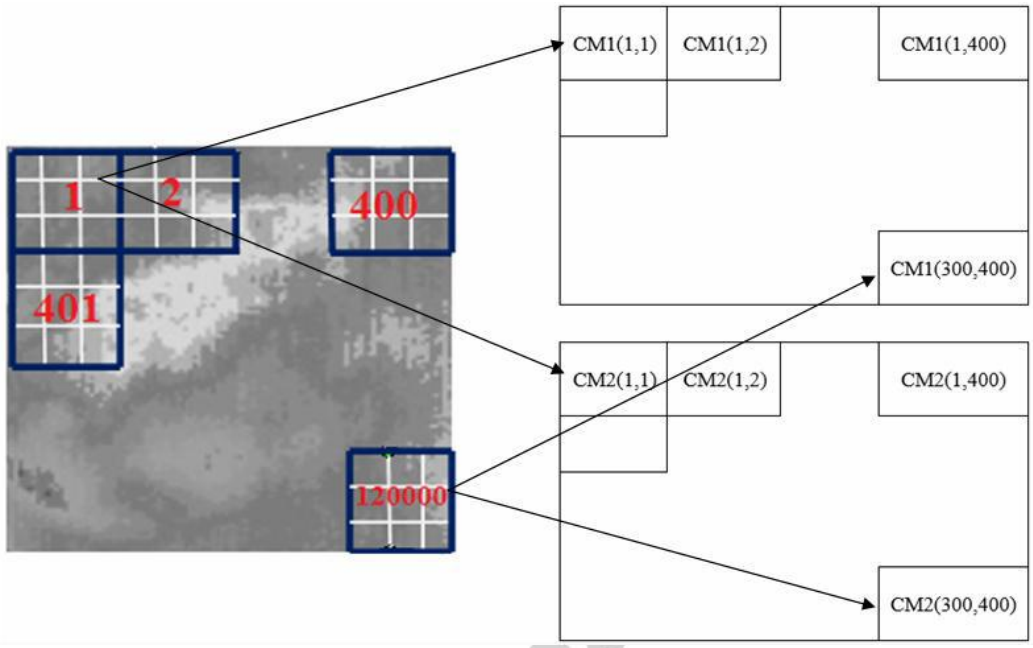

Fig. 4: Enumeration of blocks and formation of clique matrixes.

$m_{i-1,j-1}$	$m_{i,j-1}$	$m_{i+1,j-1}$
$m_{i-1,j}$	$m_{i,j}$	$m_{i+1,j}$
$m_{i-1,j+1}$	$m_{i,j+1}$	$m_{i+1,j+1}$

Fig. 5: ($m_{i,j}$) and counting direction of its eight neighbors.

200	190	201
234	198	190
212	156	209

Orginal LBP →

1	0	1
1	m_{ij}	0
1	0	1

LBPe=1+1+1+1+1+1+0=6

LBPC=1+0+1+0+1+0+1+1=5

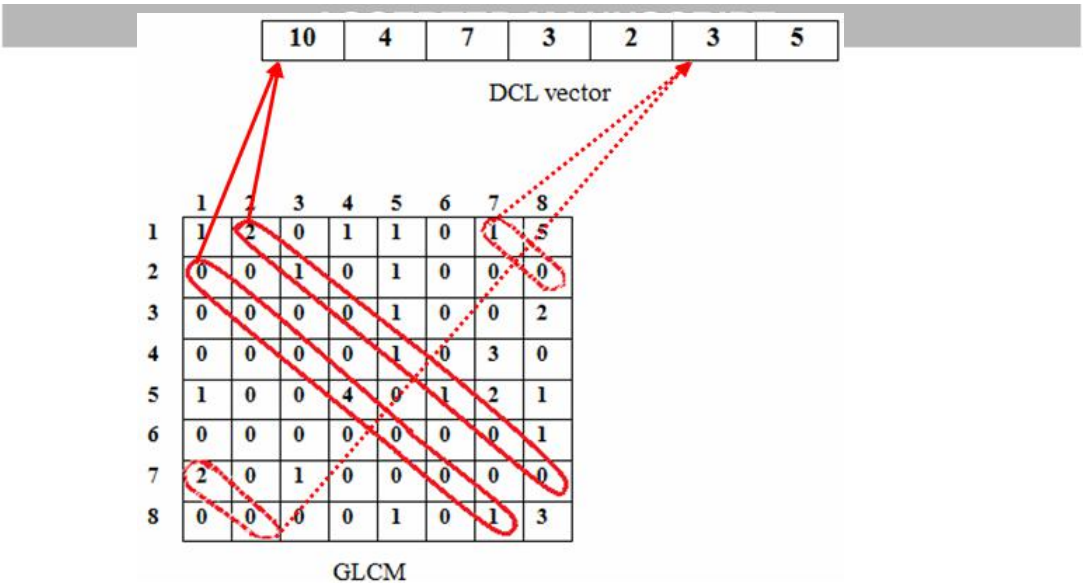

Fig. 7. The process of DCL vector extraction from GLCM.

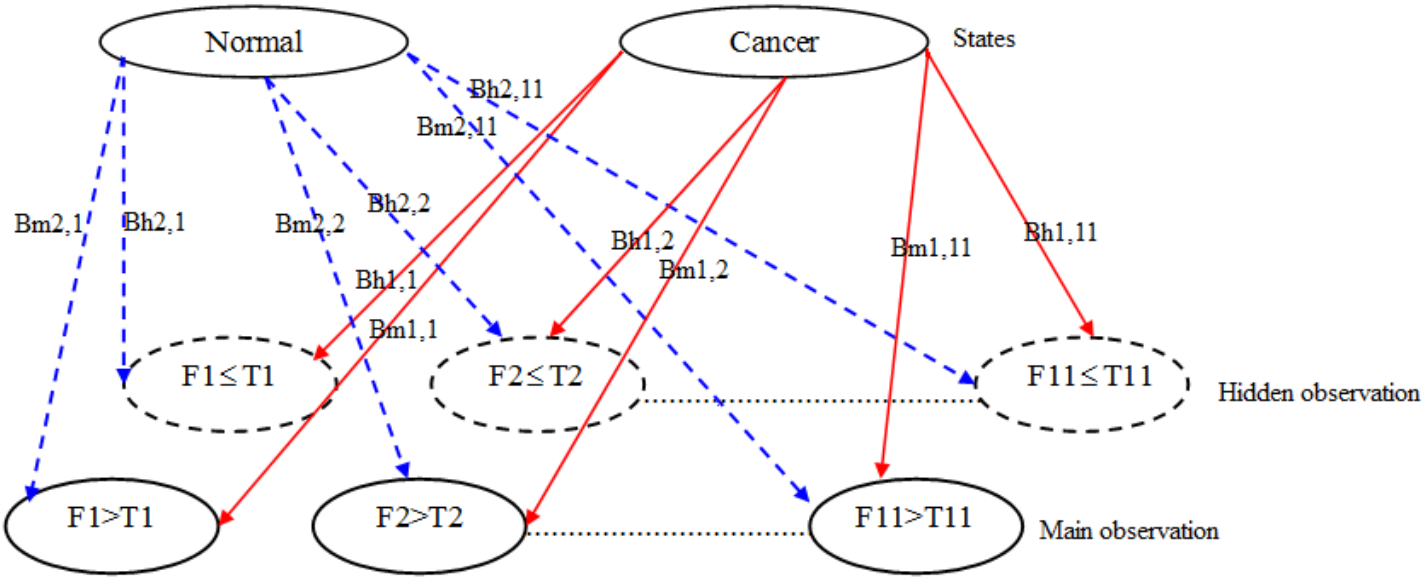

Fig. 8: Our HMM model for decision-level fusion-based classification.

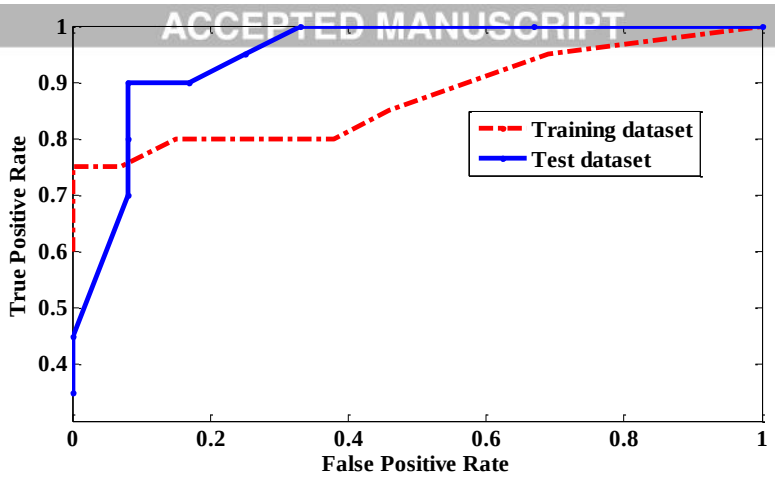

Fig. 9: ROC curves for test and training datasets.

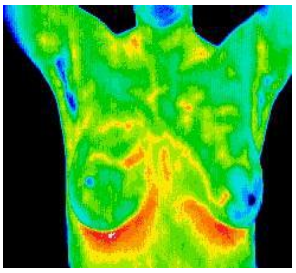

Fig. 10: A sample of normal thermography.

Table 1: Results of primitive decision by our proposed features.

Performance measures		Extracted features										
		F1 (TLBPc)	F2 (TLBPe)	F3 (DLBPc)	F4 (DLBPe)	F5 (GLBPc)	F6 (GLBPe)	F7 (LBPcs)	F8 (LBPes)	F9 (HLBPc)	F10 (HLBPe)	F11 (DGM)
Training images	TP	16	17	15	15	19	16	18	15	16	16	13
	TN	9	10	12	11	12	10	9	12	11	9	10
	FP	4	3	1	2	1	3	4	1	2	4	3
	FN	4	3	5	5	5	4	2	5	4	4	7
	TOE	8	6	6	7	6	7	6	6	6	8	10
Test images	TP	18	13	18	16	18	19	16	14	19	20	19
	TN	10	12	9	9	10	9	9	12	9	8	9
	FP	2	0	3	3	2	3	3	0	3	4	3
	FN	2	7	2	4	2	1	4	6	1	0	1
	TOE	4	7	5	7	4	4	7	6	4	4	4

TP: True Positive TN: True Negative FP: False Positive FN: False Negative TOE: Total of error

Table 2: Detection results of our decision-level fusion algorithm by means of HMM

	Performance measures								
Database	TP	TN	FP	FN	TOE	PPV	NPV	SEN	SPC
Test image	19	11	1	1	2	0.95	0.95	0.95	0.92
Training image	16	11	2	4	6	0.89	0.73	0.80	0.85

Table 3: Middle results of our decision-level fusion-based detection algorithm on six selected image samples.

Image and class	Possible observations											$P(c\|I)$	$P(n\|I)$	HMM result
	F1	F2	F3	F4	F5	F6	F7	F8	F9	F10	F11			
1.n	h	h	h	h	h	h	h	h	h	h	h	0.20	0.80	TN
2.c	m	m	m	m	m	m	m	h	m	m	m	0.78	0.22	TP
3.c	h	h	m	m	m	m	h	m	h	m	m	0.56	0.43	TP
4.n	h	h	m	m	m	h	h	h	h	m	m	0.46	0.53	TN
5.n	m	h	m	m	m	m	m	m	h	m	m	0.66	0.34	FP
6.c	h	h	h	m	m	m	h	m	h	h	h	0.40	0.60	FN

Breast Cancer Detection Using MRF-based Probable Texture Feature and Decision-level Fusion-based Classification using HMM on Thermography Images

1. We propose a two-stage breast cancer detection algorithm by decision-level fusion.

2. We tried to improve false accept of previous algorithms by our proposed algorithm.

3. We used Hidden Markov Model as a fusion algorithm to fuse primitive decisions.

4. We propose a novel texture feature based on Markov random field model.

5. To extract color and edge information of images, we modified Local Binary Pattern.